# Relationship between direct and converse piezoelectric effect in a nanoscale electromechanical contact

Sergei V. Kalinin*
*Materials Sciences and Technology Division and the Center for Nanophase Materials Sciences, Oak Ridge National Laboratory, Oak Ridge, Tennesee 37831, USA*

Boris Mirman† and Edgar Karapetian‡
*Department of Mathematics and Computer Science, Suffolk University, Boston, Massachusetts 02114, USA*
(Received 23 October 2006; revised manuscript received 17 November 2007; published 27 December 2007)

Linear piezoelectric coupling between mechanical and electrical phenomena is extremely common in inorganic and biological materials and constitutes the basis for multiple applications. In the macroscopic case, the coupling coefficients between electric displacement and strain (direct piezoeffect) and stress and electric field (converse piezoeffect) are equal, the symmetry stemming from the existence of the corresponding thermodynamic potential. Hence, studies of electromechanical coupling provide information on strain-induced polarization change, and vice versa. This is not necessarily the case for the electromechanical coupling (or any other cross-coupled property) in the contact geometry of a scanning probe microscopy or nanoindentation experiment. In this local case, the hypothetical (unknown) thermodynamic potential $\tilde{G}(P,\psi,\ldots)$ depends not only on conventional variables (e.g., load $P$ and bias $\psi$), but also on additional free length parameters, e.g. radius of contact, $a$, or indentation depth, $h$. Here we derive the relationship between the direct and converse piezoelectric effects in the contact geometry. The implications of the established relationships for nanoscale electromechanical and piezoelectric measurements are analyzed.

DOI: 10.1103/PhysRevB.76.212102 PACS number(s): 77.80.Fm, 68.37.−d, 77.65.−j

Coupling between electrical and mechanical interactions is one of the fundamental natural phenomena that underpin the functionality of an extremely broad range of materials and systems. Electromechanical interactions vary from piezoelectricity in polar noncentrosymmetric materials[1] and biopolymers[2] to flexoelectric coupling in cellular membranes and electromotor proteins in biology and molecular transformations in electrochemical reactions. In ferroelectric materials, piezoelectricity is strongly related to the electrical polarization, and can be used for high-resolution imaging of polarization distribution and probing polarization reversal processes.[3–7] In biological systems, local piezoelectric measurements can be used for high (~10 nm) resolution structural and functional imaging.[8] In organic molecules, functional electrochemical transformations can form basis for molecular electromechanical machines.[9] Furthermore, in molecular systems, origins for piezoelectricity can be traced to a single chemical bond level[10] and the properties of bulk materials are defined by relative bond orientations and collective interactions.

The ubiquity of electromechanical coupling in inorganic, macromolecular, and biological systems necessitates local quantitative studies of these phenomena. However, current detection on the sub-fA level, required to probe direct piezoelectric effect in the ~10 nm probing volume, is unfeasible. At the same time, extreme displacement sensitivity of modern atomic force microscopes and interferometers allows responses of the order of ~1–100 pm/V to be measured on the 10–30 nm length scale, providing a pathway for probing converse piezoelectric effect on the nanoscale. In the uniform field case realized in macroscopic capacitor-type measurements, the direct and converse piezoelectric effects are equal and hence the information obtained by two methods is equivalent. Here, we analyze the equality between the direct and inverse piezoelectric effects for the contact geometry of scanning probe microscopy (SPM) and nanoindentors.

In direct piezoelectric effect, the induced strain $X$ results in the electric displacement, while in converse piezoelectric effect application of an electric field $E$ results in stress $x$. The linear constitutive equations for a piezoelectric material possessing general anisotropy are

$$D_i = e_{ik}^D X_k + \varepsilon_{ij} E_j, \tag{1a}$$

$$x_k = c_{kl} X_l + e_{ki}^C E_i, \tag{1b}$$

where $X_k$ is strain, $x_l$ is stress, $D_i$ is electric displacement, $E_j$ is electric field, $c_{kl}$ are elastic stiffnesses, $e_{ik}$ are piezoelectric stress constants, and $\varepsilon_{ik}$ are dielectric constants. For spatially uniform fields, i.e., when corresponding quantities are position independent, Eqs. (1a) and (1b) allow construction of thermodynamic potential $G(X,E)$ where strain and electric field are independent variables. The coupling constants are expressed through the derivatives of the potential with respect to external parameter, e.g., $e_{ik}^C = -(\partial x_i/\partial E_k)_X$. The differential of the Gibbs free energy is $dG = -x_i dX_i - D_m dE_m$ and from the equality of mixed derivatives (Maxwell relations)

$$\left(\frac{\partial D_k}{\partial X_i}\right)_E = \left(\frac{\partial x_i}{\partial E_k}\right)_X = \left(\frac{\partial^2 G}{\partial X_i \partial E_k}\right) \tag{2}$$

the direct and converse piezoelectric coefficients are equal, $e_{ik}^D = e_{ik}^C$. Note that Eq. (2) stems directly from the fact that strain and electric fields are the only two independent state variables. The implication of Eq. (2) is that the measurements of the electromechanical response, i.e., stress generated by uniform electric field, provides information on the

 

charge produced by uniform strain, and vice versa. Both types of measurements are feasible in the macroscopic case and can be chosen depending on materials system.

Similar situation arises in the context of the problem of local electromechanical measurements using scanning probe microscopy[3] or nanoindenter[11,12] platforms. In these methods, measurement of the local electromechanical response of the surface to the bias applied to the probe or indenter is a well-established detection mechanism. The coupling coefficients as small as ~1–5 pm/V can be measured over ~10 nanometer area, providing functional basis for high-resolution imaging. At the same time, corresponding direct electromechanical coupling necessitates detection of the charges of the order of several tens of electron charge, corresponding to ~fA current at ~1 MHz, well below the detection limit of existing electronics due to fundamental limitations such as Johnson noise, and presence of stray capacitances in the circuit. Hence, macroscopic and nanoindentor-based measurements can be based on both direct[12] and converse[11] piezoelectric effects detection, while only converse electromechanical measurements are possible on the nanoscale by SPM. However, it is no longer obvious that (a) the information obtained by the two detection schemes would be equivalent even for linear piezoelectric material and (b) if additional information can be obtained through detecting both direct and converse responses.

Indeed, local probes (e.g., SPM tip or indentor) can be represented by the indentor in contact with the surface, such that indentor bias $\psi_0$ and acting load $P$ are two experimentally controlled variables, whereas generated charge $Q$ and vertical displacement $h$ are system responses. The direct and converse electromechanical responses can be defined, e.g., as $(\partial h/\partial \psi_0)_P$ and $(\partial Q/\partial P)_{\psi_0}$, respectively. However, in this case the definition of the responses is nonunique, and direct and converse responses are not necessarily equal. The reason is that in this case the contact radius $a$ (or any other length parameter defined by indenter's geometry) is an additional degree of freedom that varies in the indentation process and cannot be controlled independently. Hence thermodynamic potential $G(P,V)$ cannot be constructed in a direct fashion, nor can its existence be postulated. Below, we analyze the problem of coupled electromechanical indentation of transversely isotropic piezoelectric half-space, and derive the self-consistent descriptions for direct and converse piezoelectric effects (see Fig. 1).

For rotationally invariant indenters (Fig. 2), the contact area is a circular region with radius $a$. The mechanical boundary conditions are prescribed displacement $u_z(\rho,0)=h-w(\rho)$ in the contact area $(0\leqslant\rho\leqslant a)$, no normal pressure $\sigma_{zz}(\rho,0)=0$ outside the contact area $(\rho>a)$, and no shear traction on the surface, $\tau_z(\rho,0)=0$ for $0\leqslant\rho<\infty$. Here, $h$ specifies the total depth of penetration beneath the specimen free surface and defined as follows: $h=w_0$ for the flat and spherical indenters; $h=\varepsilon+w_0$ for the conical indenter. $w(\rho)$ specifies the shape of the tip of the indenter and defined as follows: $w(\rho)=\varepsilon(\rho/a)^2$ for spherical indenter with $\varepsilon=a^2/(2R)$, $R$ is the radius of the curvature of the tip; $w(\rho)=\varepsilon(\rho/a)$ for conical indenter with $\varepsilon=a\cot\alpha$, $\alpha$ is the semiangle of the cone measured from the apex. For both

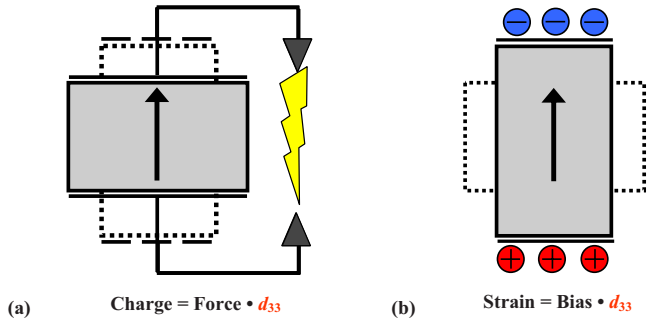


FIG. 1. (Color online) Schematic showing the (a) direct and (b) converse piezoelectric effect. In the uniform field case, corresponding coupling coefficients are equal as the consequence of the existence of thermodynamic potential. Piezoelectric strain constants are defined as $d_{nj}=e_{ni}s_{ij}$.

spherical and conical indenter $\varepsilon$ is defined as the depth of penetration measured at the circle of contact. The electrical boundary conditions are $\psi(\rho,0)=\psi_0$ for $0\leqslant\rho\leqslant a$ and $D_z(\rho,0)=0$ for $\rho>a$. The first condition implies that the indenter is a perfect electrical conductor with a constant potential $\psi_0$ prescribed at the base within the contact area, whereas the second condition tells that the electric charge distribution outside the contact area is zero.

Recently, Kalinin *et al.*[13] and Karapetian *et al.*[14,15] have obtained the exact solutions to the above-described piezoelectric indentation problems for flat, spherical and conical indenter geometries using the correspondence principle[16] in conjunction with potential theory by Fabrikant.[17,18] The stiffness relations that relate applied force $P$, concentrated charge $Q$, indenter displacement $w_0$, indenter potential $\psi_0$, indenter geometry, and material properties—for the indenters of the studied geometries have the following phenomenological structure:[14]

$$P=\frac{2}{\pi}\theta[h^{n+1}C_1+(n+1)h^n\psi_0C_3], \tag{3}$$

$$Q=\frac{2}{\pi}\theta[h^{n+1}C_2+(n+1)h^n\psi_0C_4], \tag{4}$$

where $\theta$ is geometric factor [$\theta=a$ for the flat indenter, $\theta=(2/3)\sqrt{R}$ for the spherical indenter and $\theta=(1/\pi)\tan\alpha$ for

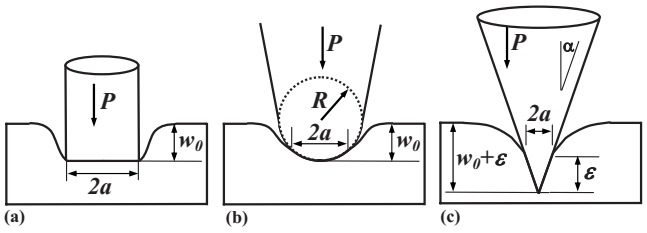


FIG. 2. Geometrical parameters for flat (a), spherical (b), and conical (c) indentation. In this case, the contact radius $a$ is an additional free parameter that can change during the experiment. Hence, no thermodynamic potential of the form $\tilde{G}(P,\psi)$ can be constructed.

the conical indenter] and $n=0$, 0.5, and 1 for the flat, spherical, and conical indenters, respectively. The constant $C_1$ and $C_4$ define elastic and dielectric responses, while $C_2$ and $C_3$ define cross-coupled responses. The constants $C_{1-4}$ entering equations (3) and (4) represent clusters of electroelastic constants introduced in Ref. 14. Hence, analysis of the relationship between direct and inverse piezoelectric effects in indentation geometry is equivalent to finding the relationship between cross-coupling constants $C_2$ and $C_3$. Originally, this equality was conjectured based on numerical analysis; here, we derive analytical proof and discuss consequences of this conjecture.

To establish this relationship, we consider the equation established in Ref. 15:

$$\frac{c_{44}+m_j(c_{13}+c_{44})+k_j(e_{15}+e_{31})}{c_{11}}=\frac{m_jc_{33}+k_je_{33}}{m_jc_{44}+(c_{13}+c_{44})+k_je_{15}}$$
$$=\frac{m_je_{33}-k_j\varepsilon_{33}}{m_je_{15}+(e_{15}+e_{31})-k_j\varepsilon_{11}}=\gamma_j^2\equiv\lambda_j, \tag{5}$$

where $c_{ij}$ denote transversely isotropic elastic stiffnesses, $e_{ij}$ piezoelectric stress constants in reduced Voigt notation, and $\varepsilon_{ij}$ are dielectric permeabilities. The constants $m_j$, $k_j$ $(j=1,2,3)$ will be given in the text to follow. By presenting Eq. (5) in the matrix form we define the following eigenvalue problem:

$$\mathbf{T}_1\mathbf{x}=\lambda\mathbf{T}_2\mathbf{x}, \tag{6}$$

where

$$\mathbf{T}_1=\begin{pmatrix} c_{44} & c_{13}+c_{44} & e_{15}+e_{31} \\ 0 & c_{33} & e_{33} \\ 0 & e_{33} & -\varepsilon_{33} \end{pmatrix},$$
$$\mathbf{T}_2=\begin{pmatrix} c_{11} & 0 & 0 \\ c_{13}+c_{44} & c_{44} & e_{15} \\ e_{15}+e_{31} & e_{15} & -\varepsilon_{11} \end{pmatrix}.$$

The eigenvalues $\lambda_j$ $(j=1,2,3)$ are found as the roots of the cubic equation in Ref. 15. Here, we consider the vector in the form of $\mathbf{x}^{(j)}=(l_j,m_j,k_j)^{tr}$, where

$$m_j=\frac{\lambda_j}{Z_j}[(c_{13}+c_{44})(\varepsilon_{33}-\lambda_j\varepsilon_{11})+(e_{33}-\lambda_je_{15})(e_{15}+e_{31})], \tag{7}$$

$$k_j=\frac{\lambda_j}{Z_j}[(c_{13}+c_{44})(e_{33}-\lambda_je_{15})-(c_{33}-\lambda_jc_{44})(e_{15}+e_{31})], \tag{8}$$

$$Z_j=(c_{33}-\lambda_jc_{44})(\varepsilon_{33}-\lambda_j\varepsilon_{11})+(e_{33}-\lambda_je_{15})^2. \tag{9}$$

$l_j=1$ if $Z_j\neq 0$, and if $Z_j=0$ then $l_j=0$ and

$$m_j=\lambda_j[(c_{13}+c_{44})(\varepsilon_{33}-\lambda_j\varepsilon_{11})+(e_{33}-\lambda_je_{15})(e_{15}+e_{31})], \tag{10}$$

$$k_j=\lambda_j[(c_{13}+c_{44})(e_{33}-\lambda_je_{15})-(c_{33}-\lambda_jc_{44})(e_{15}+e_{31})]. \tag{11}$$

Substituting $\mathbf{x}^{(j)}$ into Eq. (6), we have an identity, i.e., this vector is an eigenvector of Eq. (6) that corresponds to the eigenvalue $\lambda_j$. From the definition (Ref. 14) of $C_2$ and $C_3$ it follows that

$$C_2+C_3=\frac{1}{B^*\gamma_1\gamma_2\gamma_3}\left\{\begin{vmatrix}\gamma_1\beta_1 & \alpha_1 & k_1\\ \gamma_2\beta_2 & \alpha_2 & k_2\\ \gamma_3\beta_3 & \alpha_3 & k_3\end{vmatrix}+\begin{vmatrix}\gamma_1\beta_1 & \alpha_1 & m_1\\ \gamma_2\beta_2 & \alpha_2 & m_2\\ \gamma_3\beta_3 & \alpha_3 & m_3\end{vmatrix}\right\}. \tag{12}$$

Substitution of Eqs. (7)–(9) into the expansion of the determinants of Eq. (12) by the first columns and application of the identities $\lambda_1\lambda_2\lambda_3=D/A$ and $\lambda_1+\lambda_2+\lambda_3=B/A$, results in the equality

$$\beta_j(\alpha_{j+1}k_{j+2}-\alpha_{j+2}k_{j+1})+\alpha_j(\alpha_{j+1}m_{j+2}-\alpha_{j+2}m_{j+1})$$
$$=\frac{D(\lambda_{j+1}-\lambda_{j+2})}{c_{11}\lambda_jZ_1Z_2Z_3}(\xi\lambda_j+\eta)(A\lambda_j^3-B\lambda_j^2+C\lambda_j-D), \tag{13}$$

where the subscripts are taken modulo 3 (i.e., $\lambda_4=\lambda_1$, $\lambda_5=\lambda_2$, $\alpha_4=\alpha_1$, $\alpha_5=\alpha_2$, etc.) and

$$\xi=c_{13}[e_{15}(e_{15}+e_{31})+\varepsilon_{11}(c_{44}+c_{13})]-e_{31}(c_{44}e_{31}-c_{13}e_{15}), \tag{14}$$

$$\eta=c_{33}[e_{15}(e_{15}+e_{31})+\varepsilon_{11}(c_{44}+c_{13})]-e_{33}(c_{44}e_{31}-c_{13}e_{15}). \tag{15}$$

Since $\lambda_j$ are the roots of cubic equation in Ref. 15, the left side of Eq. (13) vanishes and therefore $C_2+C_3=0$ for any numbers $\gamma_j$ $(j=1,2,3)$. Notice that while this equality was shown numerically before, no analytical proof was available. Thus, Eqs. (3) and (4) for the indentation problem, where $C_2=-C_3$, analogously to Eqs. (1a) and (1b) retain the reciprocity, and in particular define the analog of the equality of direct and converse piezoeffects in contact geometry of SPM or nanoindentation.

Based on the demonstrated relationship $C_2=-C_3$ and stiffness relations Eqs. (3) and (4), relationships between the mixed derivatives of charge and displacement with respect to bias and force can be established in a straightforward fashion, e.g.,

$$\left(\frac{\partial Q}{\partial h}\right)_\psi=\frac{n\psi}{h}\left[1+\left(\frac{\partial\psi}{\partial P}\right)_h\right]^{-1}. \tag{16}$$

Equation (16) and similar relations allow the relating properties to be measured in the local indentation under different conditions, e.g., constant force (low frequency), constant strain (high frequency), etc. Note, however, that unlike Eq. (2) that follow from the existence of thermodynamic potential $G(X,E)$, relationships similar to Eq. (16) follow from the structure of stiffness relations Eqs. (3) and (4) and relationship $C_2=-C_3$ proven above.

We note that by setting the coupling constants $e_{ij}=0$ the problem decouples and the limiting cases of the purely elas-

tic and purely electrostatic solutions are recovered from Eqs. (3) and (4). This implies the following limits: $m_3, k_1, k_2 \to 0$, $\gamma_3 \to \sqrt{\varepsilon_{33}/\varepsilon_{11}}$. As a consequence $C_1 = H^{-1}$, where $H$ is a transversely isotropic elastic constant[17,18] and in the case of isotropic material $H = (1-\nu^2)/\pi E$, where $E$ is the elastic modulus, and $\nu$ is Poisson coefficient; $C_2 = C_3 = 0$; $C_4 = 2\pi\sqrt{\varepsilon_{11}\varepsilon_{33}}$, so that

$$P = 2\theta h^{n+1}/\pi H, \quad Q = 4a\sqrt{\varepsilon_{11}\varepsilon_{33}}\psi_0 \tag{17}$$

Hence, the capacitance for all three models is $C_{ca} = 4a\sqrt{\varepsilon_{11}\varepsilon_{33}}$.

The applicability of Eqs. (3) and (4) and derived relationships, e.g., Eq. (16) for the description of the nanoindentation and SPM experiments can be described as following. This analysis is rigorously correct for (a) linear piezoelectric materials, (b) perfectly conductive indenter, and (c) under the assumption that electrostatic field outside the contact area is negligible. For most ferroelectric materials (except, e.g., relaxors), the deviations from ideal piezoelectric behavior originate in the vicinity of the intrinsic switching thermodynamic field, $E_0 \sim P_S/\chi$, of order of $\sim 10^6 - 10^7$ V/m for most materials ($\chi$ is linear dielectric susceptibility). Estimating maximal electric field below the indenter as $\psi/a$, where $a$ (as determined form effective resolution) is $\sim 10$ nm, the deviations in behavior from ideal can start for biases as small as $\sim 1$ V (note, however, that this effect can be masked by polarization switching). For nanoindentation experiments ($a$ is $\sim 1$ $\mu$m), corresponding bias is $\sim 1$ kV (note that for nanoindentation the measurements should be performed in elastic regime). The conditions (b) and (c) can be violated for nanoscale indentor, when quantum and stray capacitance effects become important. Applicability limit for condition (b) can be estimated as $\lambda_s < a\varepsilon_g/\sqrt{\varepsilon_{11}\varepsilon_{33}}$, where $\lambda_s$ is the effective width of the ferroelectric-conductor gap (e.g., the sum of Thomas-Fermi screening length in material and ferroelectric correlation length in ferroelectric). Finally, the condition (c) corresponds to the dominance of the capacitance of tip-surface contact area vs stray tip-surface capacitance, analyzed in detail in Ref. 13 and defining the limits of weak and strong indentation in PFM.

To summarize, we have analytically established the reciprocity between direct and converse piezoelectric effects in coupled electromechanical contact of SPM or nanoindentation experiment. Unlike the macroscopic uniform field case, thermodynamic potential cannot be defined in a straightforward manner due to the presence of a third free parameter (contact radius or indentation depth), and nonhomogeneity of the electroelastic field distribution in the material. We have analyzed the physical implications of the established reciprocity principle for the nanoscale electromechanical and piezoelectric measurements.

Research supported by Division of Materials Sciences and Engineering, Oak Ridge National Laboratory, managed by UT-Battelle, LLC, for the U.S. Department of Energy. E.K. acknowledges financial support of the NSF (Grant No. CMS-0509936). E.K. and B.M. acknowledge the support from the ORNL SEED program.

*sergei2@ornl.gov
†mirman@mcs.suffolk.edu
‡edgark@mcs.suffolk.edu

[1] R. E. Newnham, *Properties of Materials: Anisotropy, Symmetry, Structure* (Oxford University Press, New York, 2005).
[2] E. Fukada, Biorheology **32**, 593 (1995).
[3] *Nanoscale Characterization of Ferroelectric Materials*, edited by M. Alexe and A. Gruverman (Springer, Berlin, 2004).
[4] *Nanoscale Phenomena in Ferroelectric Thin Films*, edited by S. Hong (Kluwer Academic, Norwell, MA, 2004).
[5] A. Gruverman, O. Auciello, and H. Tokumoto, Annu. Rev. Mater. Sci. **28**, 101 (1998).
[6] A. Gruverman and A. Kholkin, Rep. Prog. Phys. **69**, 2443 (2006).
[7] M. Molotskii, A. Agronin, P. Urenski, M. Shvebelman, G. Rosenman, and Y. Rosenwaks, Phys. Rev. Lett. **90**, 107601 (2003).
[8] S. V. Kalinin, B. J. Rodriguez, S. Jesse, T. Thundat, and A. Gruverman, Appl. Phys. Lett. **87**, 053901 (2005).
[9] V. Balzani, A. Credi, F. M. Raymo, and J. F. Stoddart, Angew. Chem., Int. Ed. **39**, 3348 (2000).
[10] A. N. Cleland, *Foundations of Nanomechanics: From Solid State Theory to Device Applications* (Springer, Berlin, 2003).
[11] A. Rar, G. M. Pharr, W. C. Oliver, E. Karapetian, and S. V. Kalinin, J. Mater. Res. **21**, 552 (2006).
[12] V. Koval, M. J. Reece, and A. J. Bushby, J. Appl. Phys. **97**, 074301 (2005).
[13] S. V. Kalinin, E. Karapetian, and M. Kachanov, Phys. Rev. B **70**, 184101 (2004).
[14] E. Karapetian, M. Kachanov, and S. V. Kalinin, Philos. Mag. **85**, 1017 (2005).
[15] E. Karapetian, I. Sevostianov, and M. Kachanov, Philos. Mag. B **80**, 331 (2000).
[16] E. Karapetian, M. Kachanov, and I. Sevostianov, Arch. Appl. Mech. **72**, 564 (2002).
[17] V. I. Fabrikant, *Applications of Potential Theory in Mechanics* (Kluwer, Dordrecht, 1989).
[18] V. I. Fabrikant, *Mixed Boundary Value problems of Potential Theory and Their Applications in Engineering* (Kluwer, Dordrecht, 1991).